Journal of Sound and Vibration (2002) **255**(2), 357–382
doi:10.1006/jsvi.2001.4159, available online at http://www.idealibrary.com on IDEAL®

ON THE FREE VIBRATION OF STIFFENED SHALLOW SHELLS

A. N. Nayak

Department of Civil Engineering, Indira Gandhi Institute of Technology, Sarang – 759 146, *Orissa, India. E-mail: nayak_an@hotmail.com*

AND

J. N. Bandyopadhyay

Department of Civil Engineering, Indian Institute of Technology, Kharagpur – 721 302, *West Bengal, India. E-mail: jnb@civil.iitkgp.ernet.in*

(*Received* 26 *June* 2001, *and in final form* 12 *November* 2001)

A finite element analysis for free vibration behaviour of doubly curved stiffened shallow shells is presented. The stiffened shell element is obtained by the appropriate combinations of the eight-/nine-node doubly curved isoparametric thin shallow shell element with the three-node curved isoparametric beam element. The shell types examined are the elliptic and hyperbolic paraboloids, the hypar and the conoidal shells. The accuracy of the formulation is established by comparing some of the authors' results of specific problems with those available in the literature. Numerical results of additional stiffened shells are also presented to study the effects of various parameters of shells and stiffeners such as orientation (i.e., along x-/y-/both x and y directions), type (concentric, eccentric at top and eccentric at bottom) and number of stiffeners, stiffener depth to shell thickness ratio, and aspect ratio, shallowness and boundary conditions of shells on free vibration characteristics.

1. INTRODUCTION

In civil engineering construction, singly curved cylindrical and doubly curved elliptic paraboloid, hyperbolic paraboloid, conoidal and hypar shells, shown in Figure 1, are commonly used as roofing units. Doubly curved shells are architecturally appealing and frequently favoured for roofing large column-free areas. Synclastic elliptic paraboloid shells are structurally stiff due to their surface geometry and can have square or rectangular planform. The anticlastic hyperbolic paraboloid, conoidal and hypar shells are ruled surfaces offering ease of casting and even penetration of natural light. These shells are often stiffened to achieve greater strength with economy of the material. However, they are frequently subjected to dynamic loadings in their service life and hence, the dynamic properties, such as natural frequencies and mode shapes, are also of primary interest to predict in-service behaviour and resonance frequencies.

During the last two decades, researchers took active interest in the dynamic behaviour of stiffened shells. Rinehart and Wang [1] investigated vibration of simply supported closed cylindrical shells with longitudinal stiffeners by employing the energy method. Mead and Bardell [2, 3] analyzed the free vibration aspects of a closed thin cylindrical shell with

0022-460X/02/$35.00

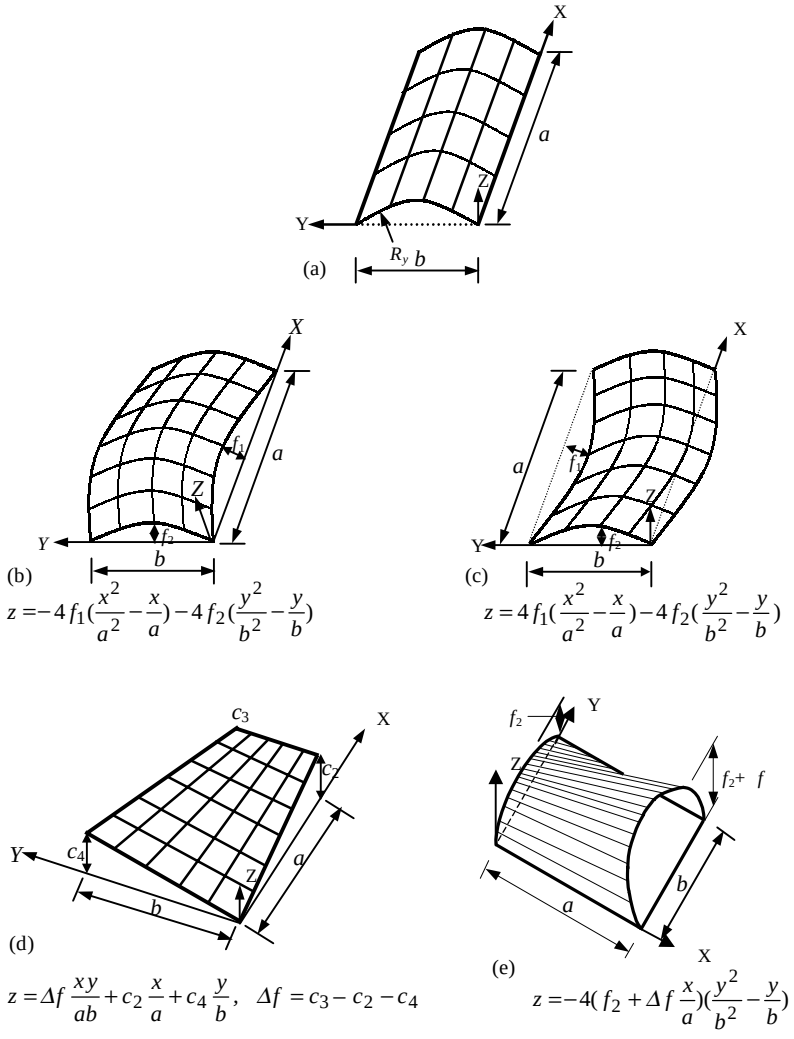

Figure 1. Types of shell forms: (a) cylindrical shell; (b) elliptic paraboloid shell; (c) hyperbolic shell; (d) hypar shell; (e) conoidal shell.

discrete axial and periodic circumferential stiffeners by wave propagation method. Mustafa and Ali [4] studied the free vibration characteristics of stiffened cylindrical shells and orthogonally stiffened cylindrically curved panels experimentally as well as numerically by employing an eight-node orthogonally stiffened super shell finite element. Mustafa and Ali [5] also applied the structural symmetry techniques with appropriate constraints on the boundaries of parts of a shell structure to the free vibration analysis of closed cylindrical and conical shells for the prediction of natural frequencies and mode shapes. Bardell and Mead [6] established the stiffness and mass matrices of a cylindrically curved rectangular panel by employing the hierarchical finite element method and then the stiffness and mass matrices are combined with periodic structure theory to analyze an orthogonally stiffened cylindrical shell with discrete line simple supports. A thin cylindrical shell stiffened axially by equi-pitched, identical stringers and circumferentially by equi-pitched, identical frames

was analyzed as a two-dimensional periodic structure by using wave propagation techniques in conjunction with the hierarchical finite element method [7]. Cheng and Dade [8] carried out the dynamic analysis of stiffened plates and shells using spline Gauss collocation method. Accrorsi and Bennett [9] applied the wave propagation techniques to a finite element model of a single periodic unit to determine the elastic wave propagation characteristics in orthogonally stiffened cylindrical shells. Mecitoglu and Dokmeci [10] investigated the free vibration analysis of thin, stiffened, shallow cylindrical shells by collocation method within the frame of the theory of classical thin orthotropic shallow shells. Langley [11] developed the dynamic stiffness technique based on a singly curved orthogonally stiffened shell element with a constant radius of curvature and simply supported along the curved edges. The same method was applied to a range of stiffened circular cylinders, a cylinder with an internal floor, and a five-panel/six stringer array. Rao *et al.* [12] investigated the natural frequencies of submerged stiffened plates/shells by using a triangular shallow shell finite element. By applying the same method, Sinha and Mukhopadhyay [13] studied the free vibration of eccentric stiffened plates/shallow shells. Further, they extended it to investigate static, free and forced vibration analyses of arbitrary non-uniform shells with tapered stiffeners [14]. Jiang and Olson [15] developed a super finite element with C^1 shell element and curved beam element for the free vibration analysis of cylindrical shells. Natural frequencies of stiffened circular cylindrical shells were investigated by Stanley and Ganesan [16] for short and long shells by semi-analytical finite element method. Sivasubramonian *et al.* [17] investigated the free vibration characteristics of longitudinally stiffened square cylindrical panels with symmetrical square cutouts using the finite element method.

It is thus seen that though, the free vibration behaviour of stiffened cylindrical shells either closed or open were studied extensively by many researchers, very less work was carried out on the free vibration characteristics of doubly curved stiffened shells. To the best of authors' knowledge, study of free vibration behaviour of doubly curved stiffened elliptic paraboloid, hyperbolic paraboloid, conoidal and hypar shells is yet to be carried out. The present work is, therefore, aimed at investigating the free vibration behaviour of the above types of stiffened shells by employing the finite element method.

2. FINITE ELEMENT FORMULATION

The element stiffness and mass matrices for the doubly curved stiffened shell element are obtained by the appropriate combinations of the eight-/nine-node doubly curved isoparametric thin shallow shell element with the three-node curved isoparametric beam element. In the present formulation, the effects of stiffness and mass of the stiffeners (three-node beam elements) are being lumped at the nodal points of the eight-/nine-node shell elements; thereby, it is possible and convenient to position the beam element at any desired location along x or y direction with respect to the overall shell element geometry and nodal configurations. If required, the beam elements used as stiffeners can be placed even at arbitrary locations irrespective of the presence of shell element nodes.

2.1. SHELL ELEMENT

A doubly curved thin shallow shell of uniform thickness h made of homogeneous, isotropic, linearly elastic material is considered. The radii of curvature of the shell along

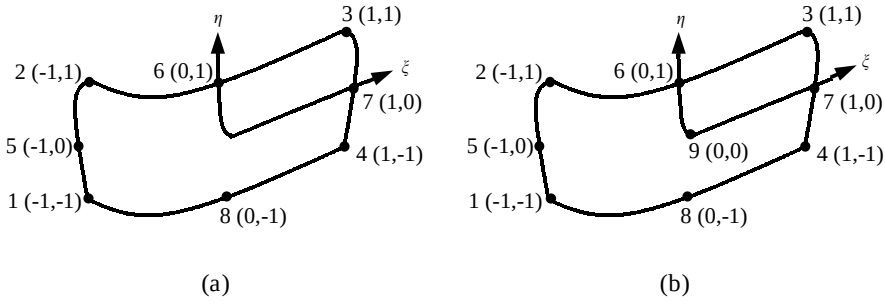

Figure 2. Doubly curved isoparametric shell elements: (a) eight-node (N8); (b) nine-node (N9).

x and y directions are R_x and R_y, respectively, and the twist radius of curvature is taken as R_{xy}. The projection of the shell on the xy plane is a rectangle of dimensions a and b. The equation of the middle surface of the shell, referred to a system of orthogonal axes (x, y, z), may be expressed as

$$z = f(x, y). \tag{1}$$

A shell is characterized as shallow if any infinitesimal line element of its middle surface may be approximated by the length of its projection on the xy plane. This implies that

$$\left(\frac{\partial z}{\partial x}\right)^2 \ll 1, \quad \left(\frac{\partial z}{\partial y}\right)^2 \ll 1, \quad \left(\frac{\partial z}{\partial x}\right)\left(\frac{\partial z}{\partial y}\right) \ll 1. \tag{2}$$

Moreover, the lateral boundary of a shallow shell may be approximated by its projection on the xy plane with regard to its boundary conditions. According to Vlasov [18], the above conditions are practically satisfied for shells with a rise-to-span ratio less than $\frac{1}{5}$.

The eight-node (N8) and nine-node (N9) doubly curved isoparametric thin shell elements, as shown in Figure 2, are used here with 5 degrees of freedom (d.o.f.s.) at each node. It includes three displacements, u, v and w along x-, y- and z-axis, respectively, and two rotations, α and β along x- and y-axis respectively. The analysis of shells is based on the modified Sanders' first approximation theory for thin shells.

The displacements at any point, with isoparametric coordinates ξ and η, are related to the nodal d.o.f.s. by

$$u = \sum_1^n N_i u_i, \quad v = \sum_1^n N_i v_i, \quad w = \sum_1^n N_i w_i,$$

$$\alpha = \sum_1^n N_i \alpha_i, \quad \beta = \sum_1^n N_i \beta_i, \tag{3}$$

where i and n are the corresponding and total number of nodes in a shell element, and N_i is the usual shape function of the ith node.

In the isoparametric formulation the element geometry is also defined by the same shape functions, i.e.,

$$x = \sum_1^n N_i x_i, \quad y = \sum_1^n N_i y_i. \tag{4}$$

The constitutive relations for the shell element are

$$\{F\} = [D]\{\varepsilon\}, \tag{5}$$

where

$$\{F\} = [N_x, N_y, N_{xy}, M_x, M_y, M_{xy}, Q_{xz}, Q_{yz}]^{\mathrm{T}}, \tag{6}$$

$$\{\varepsilon\} = [\varepsilon_x^0, \varepsilon_y^0, \gamma_{xy}^0, k_x, k_y, k_{xy}, \gamma_{xz}^0, \gamma_{yz}^0]^{\mathrm{T}}. \tag{7}$$

Here, N_x, N_y, N_{xy}, M_x, M_y, M_{xy}, Q_{xz} and Q_{yz} are the usual force, moment and shear resultants, ε_x^0, ε_y^0, γ_{xy}^0, γ_{xz}^0 and γ_{yz}^0 are mid-surface usual axial and shear strains, and k_x, k_y and k_{xy} are the curvatures.

$[D]$ is the elasticity matrix and expressed as follows:

$$[D] = \begin{bmatrix} D_{XA} & D_{IA} & 0 & 0 & 0 & 0 & 0 & 0 \\ D_{IA} & D_{YA} & 0 & 0 & 0 & 0 & 0 & 0 \\ 0 & 0 & D_{XYA} & 0 & 0 & 0 & 0 & 0 \\ 0 & 0 & 0 & D_{XF} & D_{IF} & 0 & 0 & 0 \\ 0 & 0 & 0 & D_{IF} & D_{YF} & 0 & 0 & 0 \\ 0 & 0 & 0 & 0 & 0 & D_{XYF} & 0 & 0 \\ 0 & 0 & 0 & 0 & 0 & 0 & S_X & 0 \\ 0 & 0 & 0 & 0 & 0 & 0 & 0 & S_Y \end{bmatrix}, \tag{8}$$

where

$$D_{XA} = D_{YA} = \frac{Eh}{(1-\nu^2)}, \quad D_{XYA} = \frac{Eh}{2(1+\nu)}, \quad D_{XF} = D_{YF} = \frac{Eh^3}{12(1-\nu^2)},$$

$$D_{IA} = \nu D_{XA}, \quad D_{IF} = \nu D_{XF}, \quad D_{XYF} = \frac{1-\nu}{2} D_{XF}, \quad S_X = S_Y = \frac{Eh}{2\alpha(1+\nu)}, \tag{9}$$

α is the factor to account for the non-uniform shear strain distribution across the thickness of the plate/shell and approximately taken as 1·2 for the rectangular, homogeneous section and corresponds to a parabolic shear stress distribution [19].

On the basis of the first order shear deformation theory of thin shells, the strain–displacement relations are specialized for shallow shells as follows:

$$\begin{Bmatrix} \varepsilon_x^0 \\ \varepsilon_y^0 \\ \gamma_{xy}^0 \\ k_x \\ k_y \\ k_{xy} \\ \gamma_{xz}^0 \\ \gamma_{yz}^0 \end{Bmatrix} = \begin{Bmatrix} \dfrac{\partial u}{\partial x} - \dfrac{w}{R_x} \\ \dfrac{\partial v}{\partial y} - \dfrac{w}{R_y} \\ \dfrac{\partial u}{\partial y} + \dfrac{\partial v}{\partial x} - \dfrac{2w}{R_{xy}} \\ \dfrac{\partial \alpha}{\partial x} \\ \dfrac{\partial \beta}{\partial y} \\ \dfrac{\partial \alpha}{\partial y} + \dfrac{\partial \beta}{\partial x} \\ \alpha + \dfrac{\partial w}{\partial x} \\ \beta + \dfrac{\partial \beta}{\partial y} \end{Bmatrix}. \tag{10}$$

The element stiffness and mass matrices are derived on the basis of minimum energy principle. The element stiffness matrix is given by

$$[K_{she}] = \iint [B]^{\mathrm{T}} [D][B] \, \mathrm{d}x \, \mathrm{d}y. \tag{11}$$

The element mass matrix is obtained as

$$[M_{she}] = \iint [N]^{\mathrm{T}} [P][N] \, \mathrm{d}x \, \mathrm{d}y, \tag{12}$$

where $[B]$ contains the local derivatives of shape functions and $[N]$ is the shape function matrix.

The inertia matrix $[P]$ is obtained as follows:

$$[P] = \begin{bmatrix} \rho h & 0 & 0 & 0 & 0 \\ 0 & \rho h & 0 & 0 & 0 \\ 0 & 0 & \rho h & 0 & 0 \\ 0 & 0 & 0 & \dfrac{\rho h^3}{12} & 0 \\ 0 & 0 & 0 & 0 & \dfrac{\rho h^3}{12} \end{bmatrix}. \tag{13}$$

The element stiffness and mass matrices are first evaluated by expressing the integrals in local natural co-ordinates of the element and then performing 2×2 reduced numerical integration by using the Gaussian quadrature to avoid shear locking.

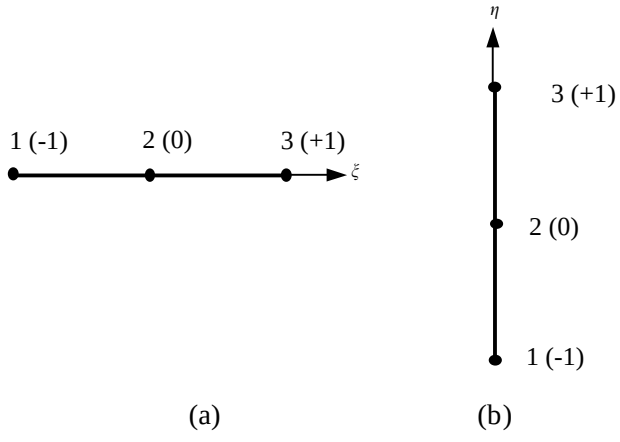

Figure 3. Three-node isoparametric curved stiffener elements: (a) x-stiffener; (b) y-stiffener.

2.2. STIFFENER ELEMENT

The shape functions of three-node curved isoparametric beam element for x and y directional stiffeners as shown in Figures 3(a) and 3(b), respectively, are taken as considered by Deb and Booton [20] and are expressed as follows:

For x-stiffeners:

$$N_{\xi i} = 0{\cdot}5\xi\xi_i(1 + \xi\xi_i) \quad \text{for } i = 1, 3, \tag{14}$$

$$N_{\xi i} = (1 - \xi^2) \quad \text{for } i = 2. \tag{15}$$

For y-stiffeners:

$$N_{\eta i} = 0{\cdot}5\eta\eta_i(1 + \eta\eta_i) \quad \text{for } i = 1, 3, \tag{16}$$

$$N_{\eta i} = (1 - \eta^2) \quad \text{for } i = 2. \tag{17}$$

In the stiffener element, each node is having 4 d.o.f., u_{sx}, w_{sx}, α_{sx} and β_{sx} for x-stiffener and v_{sy}, w_{sy}, α_{sy} and β_{sy} for y-stiffener. The displacement field at any point can be expressed in terms of nodal displacements as follows:

$$\{\delta_{sx}\} = [N_{\xi i}]\{\delta_{sxi}\} \quad \text{for } x\text{-stiffener}, \tag{18}$$

$$\{\delta_{sy}\} = [N_{\eta i}]\{\delta_{syi}\} \quad \text{for } y\text{-stiffener}, \tag{19}$$

where

$$\{\delta_{sxi}\} = [u_{sx1}\ \ w_{sx1}\ \ \alpha_{sx1}\ \ \beta_{sx1}\ \ \cdots\ \ u_{sx3}\ \ w_{sx3}\ \ \alpha_{sx3}\ \ \beta_{sx3}]^{\mathrm{T}}, \tag{20}$$

$$\{\delta_{syi}\} = [v_{sy1}\ \ w_{sy1}\ \ \alpha_{sy1}\ \ \beta_{sy1}\ \ \cdots\ \ v_{sy3}\ \ w_{sy3}\ \ \alpha_{sy3}\ \ \beta_{sy3}]^{\mathrm{T}}. \tag{21}$$

The generalized constituent relation for x-directional stiffener can be expressed as

$$\{F_{sx}\} = [D_{sx}]\{\varepsilon_{sx}\} = [D_{sx}][B_{sx}]\{\delta_{sxi}\}, \tag{22}$$

where

$$\{F_{sx}\} = [N_{sxx}\ \ M_{sxx}\ \ T_{sxx}\ \ Q_{sxz}]^{\mathrm{T}}, \tag{23}$$

$$\{\varepsilon_{sx}\} = [u_{sx,x}\ \ \alpha_{sx,x}\ \ \beta_{sx,x}\ \ (\alpha_{sx} + w_{sx,x})]^{\mathrm{T}}. \tag{24}$$

Here, N_{sxx}, M_{sxx}, T_{sxx} and Q_{sxxz} are usual axial force, moment, torsion and shear resultant of x-stiffener element. The elasticity matrix of x-stiffener element $[D_{sx}]$ is obtained as follows:

$$[D_{sx}] = \begin{bmatrix} E_{sx}A_{sx} & E_{sx}S_{sx} & 0 & 0 \\ E_{sx}S_{sx} & E_{sx}I_{sx} & 0 & 0 \\ 0 & 0 & G_{sx}J_{sxe} & 0 \\ 0 & 0 & 0 & \dfrac{G_{sx}A_{sx}}{1{\cdot}5} \end{bmatrix}, \tag{25}$$

where E_{sx}, G_{sx}, A_{sx}, S_{sx}, I_{sx} and J_{sxe} are the modulus of elasticity, modulus of rigidity, cross-sectional area, first moment of area, moment of inertia about the reference axis and equivalent polar moment of inertia of the isotropic x-stiffener respectively.

The effect of eccentricity of the x-stiffener, e_{sx} with respect to the mid-surface of the shell can be included automatically by considering the mid-surface of the shell as the reference axis for the calculation of sectional parameters of the stiffeners.

The effect of curvature of the x-stiffener can be considered as follows:

$$u_{sxi} = \left(1 + \frac{e_{sx}}{R_x}\right) u_i, \quad v_{sxi} = v_i, \quad w_{sxi} = w_i, \quad \alpha_{sxi} = \alpha_i, \quad \beta_{sxi} = \beta_i. \tag{26}$$

Hence, the transformation matrix for curvature effect of x-stiffener can be written as

$$[T_{csx}] = \begin{bmatrix} 1 + \dfrac{e_{sx}}{R_x} & 0 & 0 & 0 & 0 \\ 0 & 1 & 0 & 0 & 0 \\ 0 & 0 & 1 & 0 & 0 \\ 0 & 0 & 0 & 1 & 0 \\ 0 & 0 & 0 & 0 & 1 \end{bmatrix}. \tag{27}$$

The displacements at the nodal points of x-stiffener with respect to mid-surface of shell element can be transferred to the shell nodal points with the relation given by

$$\sum_{1}^{3} \delta_i = \sum_{1}^{n} N_i [I] \{\delta_i\} = [T_{sh}] \{\delta_i\}. \tag{28}$$

From equations (26) and (28), the nodal displacement of the x-stiffener can be obtained as follows:

$$\{\delta_{sxi}\} = [T_{sx}] \{\delta_i\}, \tag{29}$$

where

$$[T_{sx}] = [T_{csx}][T_{sh}]. \tag{30}$$

The element stiffness and mass matrices of x-stiffener can be obtained as

$$[K_{xe}] = \int [T_{sx}]^{\mathrm{T}} [B_{sx}]^{\mathrm{T}} [D_{sx}][B_{sx}][T_{sx}]\,\mathrm{d}x, \tag{31}$$

$$[M_{xe}] = \int [T_{sx}]^{\mathrm{T}} [N_{sx}]^{\mathrm{T}} [P_{sx}][N_{sx}][T_{sx}]\,\mathrm{d}x, \tag{32}$$

where $[N_{sx}]$ is the shape function matrix and $[P_{sx}]$ is the inertia matrix of the x-stiffener.

The element stiffness and mass matrices are first evaluated by expressing the integrals in local natural co-ordinate, ξ of the element and then performing 2×2 reduced numerical integration by using Gaussian quadrature. The element stiffness $[K_{ye}]$ and mass $[M_{ye}]$ matrices for the y-stiffener can be obtained in a similar manner as for the x-stiffener. Then, the element stiffness and mass matrices for the stiffened shell is given by

$$[K_e] = [K_{she}] + [K_{xe}] + [K_{ye}], \tag{33}$$

$$[M_e] = [M_{she}] + [M_{xe}] + [M_{ye}]. \tag{34}$$

The element matrices are then assembled to obtain the global $[K]$ and $[M]$ matrices. The standard eigenvalue problem for the undamped free vibration takes the form:

$$[K]\{d\} = \omega^2 [M]\{d\}, \tag{35}$$

where ω is the natural frequency in radian per second and $\{d\}$ represents eigenvectors. Equation (35) is solved by subspace iteration algorithm to determine the natural frequencies and mode shapes.

3. NUMERICAL RESULTS AND DISCUSSIONS

The accuracy of the present formulations (N8 and N9) is first established by comparing the present free vibration results of various unstiffened shell problems with those of earlier investigators available in the literature. It is worth mentioning that the authors failed to get the free vibration results of stiffened hyperbolic paraboloid, hypar and conoidal shells from the available literature. Non-dimensional fundamental frequencies $[\varpi = \omega(ab/h)\sqrt{\rho/E}]$ of shallow unstiffened elliptic paraboloid, hyperbolic paraboloid, hypar and conoidal shells obtained by N8 and N9 formulations are presented in Table 1, along with those obtained by Stavridis [21]. The edges of the above shells are supported either by simple support (S_BS_M) or by support fixed against rotation (C_BS_M) as in the literature [21]. The results compare extremely well for both the formulations.

To validate the present formulations for stiffened plates as a special case and stiffened shallow shells, the natural frequencies of three numerical problems, such as a clamped square plate with central stiffener (Figure 4), clamped as well as cantilever cylindrical shells with longitudinal stiffeners (Figure 5) and a cross-stiffened simply supported spherical shell (Figure 6), are presented in Tables 2–4, respectively, along with the results available in the respective literature [12, 17, 22–24]. Deviations of the present results from those obtained by the earlier researchers are negligible justifying good agreement for all the above problems and hence, the formulations are validated.

The convergence study of both the elements (N8 and N9) is carried out with respect to mesh size for the elliptic paraboloid shell stiffened with one central stiffener along x and y directions with simply supported (SS) and clamped (CC) boundary conditions and

TABLE 1

Non-dimensional fundamental frequency $[\varpi = \omega(ab/h)\sqrt{\rho/E}]$ *for shallow shells* ($\nu = 0{\cdot}15$)

Shell form	Boundary condition	$\varepsilon = ab/h^2$	Shallowness parameters	b/a	Stavridis [21]	Present FEM results N8	Present FEM results N9
Elliptic paraboloid	S_BS_M-S_BS_M/ S_BS_M-S_BS_M	10 000	$f_1/a = 0{\cdot}05$ $f_2/b = 0{\cdot}05$	0·50 1·00	34·697 40·413	34·122 39·808	34·126 39·809
	C_BS_M-C_BS_M/ C_BS_M-C_BS_M	10 000	$f_1/a = 0{\cdot}05$ $f_2/b = 0{\cdot}05$	0·50 1·00	36·840 41·355	36·311 40·775	36·283 40·762
Hyperbolic paraboloid	S_BS_M-S_BS_M/ S_BS_M-S_BS_M	10 000	$f_1/a = 0{\cdot}05$ $f_2/b = 0{\cdot}05$	0·50 1·00	13·413 5·763	13·160 5·763	13·162 5·763
	C_BS_M-C_BS_M/ C_BS_M-C_BS_M	10 000	$f_1/a = 0{\cdot}05$ $f_2/b = 0{\cdot}05$	0·50 1·00	18·838 11·928	18·600 11·801	18·544 11·727
Hypar	S_BS_M-S_BS_M/ S_BS_M-S_BS_M	10 000	$\Delta f/a = 0{\cdot}15$ $\Delta f/a = 0{\cdot}20$	1·00 1·00	15·316 15·921	15·276 15·844	15·272 15·839
		20 000	$\Delta f/a = 0{\cdot}15$ $\Delta f/a = 0{\cdot}20$	1·00 1·00	15·223 16·080	15·215 16·052	15·210 16·040
Conoidal	S_BS_M-S_BS_M/ S_BS_M-S_BS_M	10 000	$f_2/b = 0{\cdot}00$ $\Delta f/b = 0{\cdot}10$ $f_2/b = 0{\cdot}00$ $\Delta f/b = 0{\cdot}20$ $f_2/b = 0{\cdot}00$ $\Delta f/b = 0{\cdot}10$ $f_2/b = 0{\cdot}00$ $\Delta f/b = 0{\cdot}20$	0·50 0·50 1·0 1·0	10·870 14·990 13·659 18·590	10·817 14·795 13·612 18·387	10·811 14·752 13·590 18·276

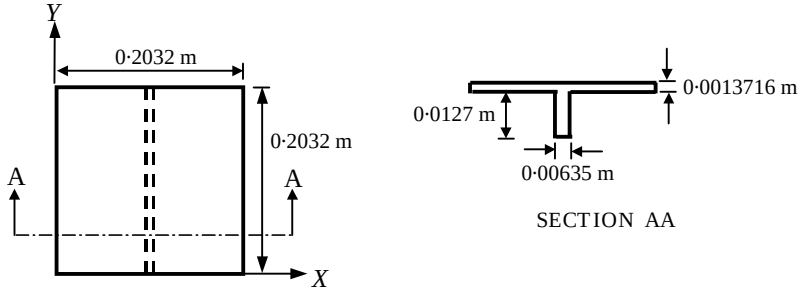

Figure 4. Clamped square plate with one central stiffener: $E = 6{\cdot}87 \times 10^{10}$ N/m^2, $\nu = 0{\cdot}29$, $\rho = 2823$ kg/m^3.

presented in Figure 7. It is observed that the non-dimensional fundamental frequencies

$$[\varpi = \omega b^2 \{12\rho(1 - \nu^2)/(Eh^2)\}^{1/2}]$$

of both the elements are converged to nearly the same value. But, the rate of convergence in nine-node shell element is faster than the other one. The results of the simply supported stiffened shell converge faster at 8×8 mesh size while, those with clamped ones converge at 16×16 mesh size. Hence, the nine-node shell element is considered with 8×8 and 16×16

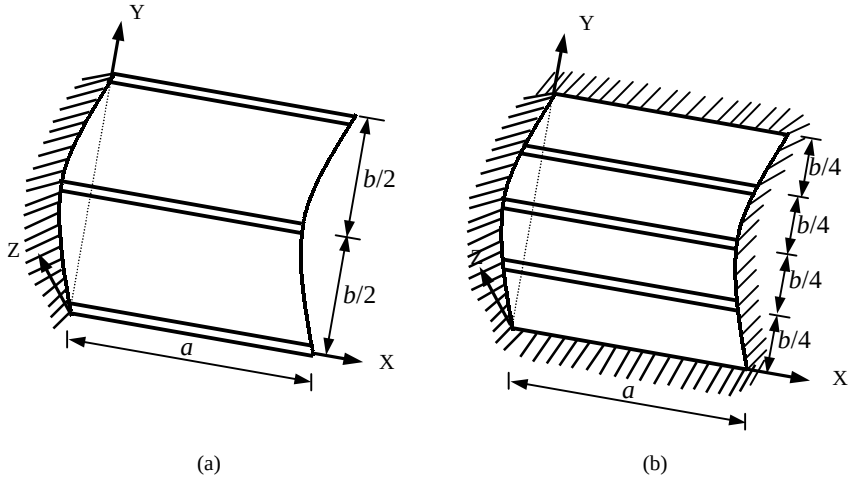

Figure 5. Stiffened cylindrical shell: (a) cantilever panel; (b) clamped panel.

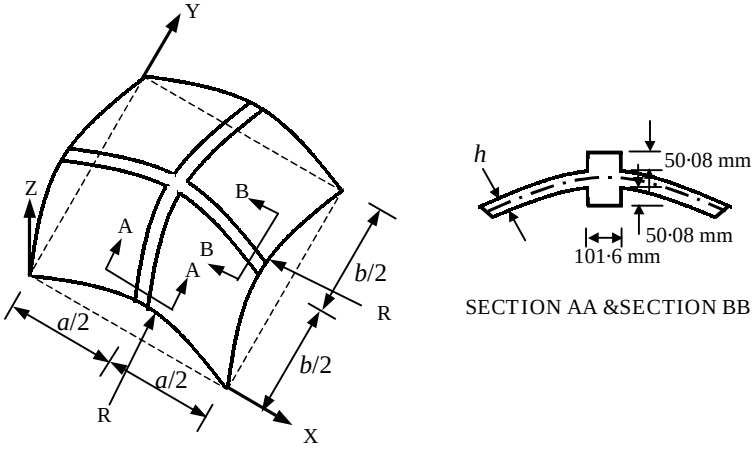

Figure 6. Simply supported concentrically stiffened spherical shell: $a = b = 1{\cdot}5698$ m, $R = 2{\cdot}54$ m, $h = 99{\cdot}451$ mm, $\rho = 7728{\cdot}97$ kg/m^3, $E = 68{\cdot}9 \times 10^6$ N/m^2, $\nu = 0{\cdot}30$.

mesh sizes for the simply supported and clamped stiffened shells, respectively, for further numerical studies.

Several additional examples of four typical doubly curved shallow shells including elliptic paraboloid, hyperbolic paraboloid, hypar and conoidal shells are judiciously chosen with respect to their aspect ratio ($\gamma = a/b$), boundary condition and shallowness parameter (λ, defined later) and having stiffeners up to 10 in number. The stiffeners are having three different orientations (along x, y and orthogonal, i.e., along both x and y directions) and three different types (concentric, eccentric at top and eccentric at bottom). Moreover, the examples have one constant/varying non-dimensional parameter d_{st}/h (stiffener depth to shell thickness ratio), in addition to the following constant non-dimensional parameters:

$$b/h = 250, \quad b_{st}/h = 2 \quad \text{and} \quad \nu = 0{\cdot}15 \quad \text{for all the above shells,}$$

$$R_y/R_x = 1{\cdot}0 \quad \text{and} \quad R_y/b = 3 \quad \text{for elliptic paraboloid,}$$

TABLE 2

Natural frequencies (Hz) of centrally stiffened clamped square plate (Figure 4)

Mode no.	Olson and Hazell [22] Test	Olson and Hazell [22] Theory (FEM)	Mukherjee and Mukhopadhyay [23] (FEM)	Bhimaraddi *et al.* [24] (FEM)	Sivasubramonian *et al.* [17] (FEM)	Present results N8 (FEM)	Present results N9 (FEM)
1	689	718·1	711·8	700·4	729·6	725·2	725·1
2	725	751·4	768·2	737·0	748·0	745·3	745·2
3	961	997·4	1016·5	966·6	1009·1	987·6	987·1
4	986	1007·1	1031·9	—	1016·6	994·4	993·9
5	1376	1419·8	1465·2	1380·1	1321·8	1401·9	1400·4

TABLE 3

Natural frequencies (Hz) of stiffened cylindrical shells for various radius of curvatures. (Figure 5, Shell: $a = b = 500$ mm, $h = 1{\cdot}4$ mm, $E = 1{\cdot}71 \times 10^{11}$ N/m^2, $\rho = 7430$ kg/m^3, $\nu = 0{\cdot}3$; Stiffener: I-section, flange width = 15 mm, flange thickness = 2 mm, web thickness = 2 mm, height of the section = 24 mm, $E_s = 2{\cdot}1 \times 10$ N/m^2, $\rho_s = 7430$ kg/m^3, $\nu_s = 0{\cdot}3$)

R (mm)	Mode no.	Cantilever (C–F–F–F) Sivasubramonian *et al.* [17]	Cantilever (C–F–F–F) Present FEM results N8 (12 × 12)	Cantilever (C–F–F–F) Present FEM results N9 (8 × 8)	Clamped (C–C–C–C) Sivasubramonian *et al.* [17]	Clamped (C–C–C–C) Present FEM results N8 (20 × 20)	Clamped (C–C–C–C) Present FEM results N9 (16 × 16)
Plate	1	67·3	68·4	68·4	350·8	342·5	342·6
	2	68·4	68·6	68·6	382·5	372·7	373·0
	3	115·9	119·8	119·5	426·2	414·1	414·6
	4	121·5	120·1	119·9	428·9	416·2	416·7
	5	130·9	127·9	127·2	461·6	447·3	446·5
2000	1	68·1	66·7	66·7	356·9	347·9	347·9
	2	74·3	75·2	75·2	401·3	390·3	390·5
	3	131·3	132·6	132·6	464·6	449·5	450·0
	4	134·2	138·1	138·2	474·4	460·4	459·5
	5	166·5	162·3	161·8	507·8	493·7	492·9
500	1	82·0	83·7	83·6	412·9	399·8	399·9
	2	87·1	89·8	89·8	525·3	506·7	507·0
	3	156·5	155·7	155·8	640·4	615·3	614·4
	4	183·2	184·2	184·7	765·3	746·5	747·5
	5	265·8	265·6	269·1	772·7	749·5	751·5

$R_y/R_x = -1{\cdot}0, \quad R_y/b = 3$ for hyperbolic paraboloid,

$\Delta f/b = 0{\cdot}2$ for hypar shells,

$(f_2 + \Delta f)/b = 0{\cdot}15$ and $f_2/(f_2 + \Delta f) = 0{\cdot}25$ for conoidal shell.

All the symbols are either defined in Appendix A or shown in Figure 1.

TABLE 4

Natural frequency (rad/s) of simply supported spherical shell with concentric orthogonal stiffeners (Figure 6)

Mode number	Rao *et al.* [12]		Present results			
			N8		N9	
	4×4 mesh	8×8 mesh	4×4 mesh	8×8 mesh	4×4 mesh	8×8 mesh
1	41·05	41·08	40·27	40·26	40·27	40·26
2	74·77	74·68	71·79	70·98	71·63	70·97
3	75·26	74·74	71·79	70·98	71·63	70·97
4	100·49	98·99	98·49	96·06	97·24	96·06

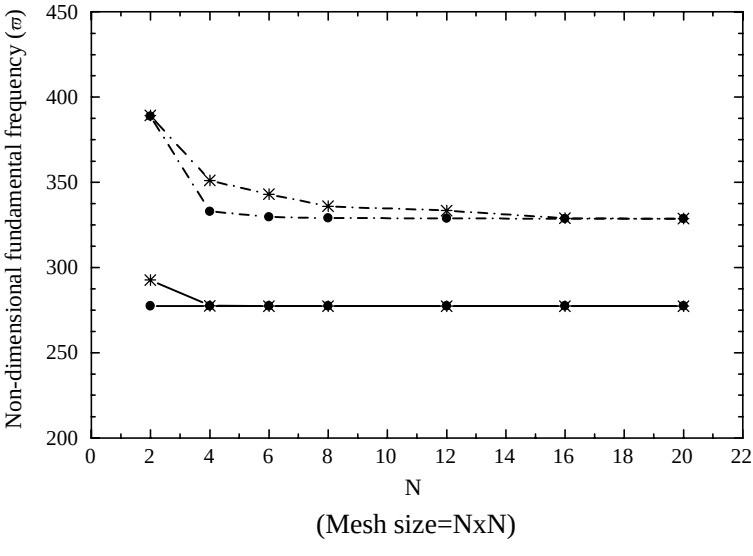

Figure 7. Convergence study of shell elements (N8 and N9) of elliptic paraboloid shell with one central stiffener in each orthogonal direction. —∗—, N8 (SS); —●—, N9 (SS); –·∗–·, N8 (CC); –·●–· N9 (CC).

The orthogonal stiffeners are placed in such a manner that the location of the same can be defined with respect to global co-ordinates as follows:

For x-stiffeners:

$$y_i = \frac{b}{(n_x + 1)}\, i \quad \text{for } i = 1, 2, 3, \ldots, n_x. \tag{36}$$

For y-stiffeners:

$$x_i = \frac{a}{(n_y + 1)}\, i \quad \text{for } i = 1, 2, 3, \ldots, n_y. \tag{37}$$

The shallowness parameter (λ) of different shell forms, according to Stavridis [21], is as follows:

TABLE 5

Details of constant/varying non-dimensional parameters both for shells and stiffeners of different types of numerical problems along with the location of their respective results

Sl. no.	Shell parameters			Stiffener parameters			Combined parameters (d_{st}/h)	Results and their locations
	$\gamma = a/b$	Boundary condition	λ	Number	Orientation	Type		
1	1·0	Clamped	—	Up to 10×10	All three	All three	6	ϖ versus number of stiffeners in Figures 8–11
2	2·0, 1·0 and 0·5	Simply supported and clamped	—	Up to 10×10	Orthogonal	Eccentric at top	6	ϖ versus number of stiffeners in Figures 12–15
3	1·0	Clamped	—	Up to 10×10	Orthogonal	Eccentric at top	Up to 20	ϖ versus (d_{st}/h) in Figures 16–19
4	1·0	Simply supported and clamped	Up to 0·2	Only 4×4	Orthogonal	Eccentric at top	6	ϖ versus λ in Figures 20 and 21

For elliptic paraboloid shell:

$$\lambda = \frac{f_1}{a} + \frac{1}{\gamma}\left(\frac{f_2}{b}\right). \tag{38}$$

For hyperbolic paraboloid shell:

$$\lambda = \max\left[\frac{f_1}{a}, \frac{f_2}{b}\right]. \tag{39}$$

For hypar shell:

$$\lambda = \frac{\Delta f}{b}. \tag{40}$$

For conoidal shell:

$$\lambda = \frac{f_2}{b} + \frac{f_2 + \Delta f}{b}. \tag{41}$$

If the shallowness parameter (λ) of any shell is limited to 0·2, the condition of shallow shell is satisfied. It is worth mentioning that the shallowness parameter (λ) of all the shells considered in the numerical problems is limited to 0·2.

In addition to the constant non-dimensional parameters mentioned above for the different examples, other constant/varying non-dimensional parameters both for the shells and stiffeners are presented in Table 5 as a ready reference, along with the location of their respective results of non-dimensional fundamental frequencies (ϖ).

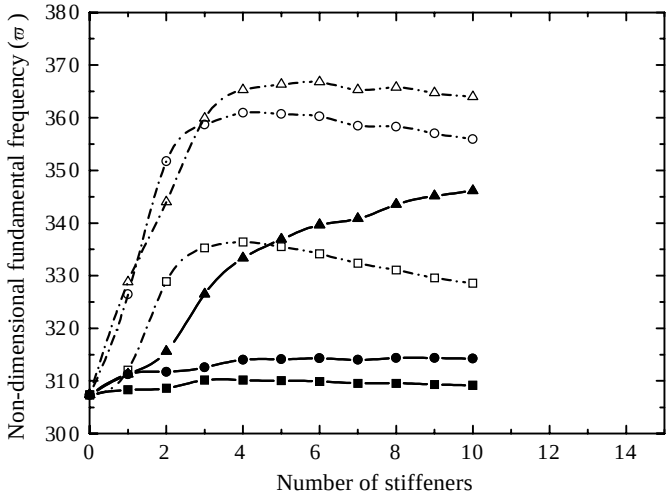

Figure 8. Variation of non-dimensional fundamental frequency of stiffened clamped elliptic paraboloid shell with respect to numbers, types and orientations of stiffeners ($\gamma = a/b = 1$, $b/h = 250$, $R_y/R_x = 1$, $R_y/b = 3$, $b_{st}/h = 2$, $d_{st}/h = 6$ and $\nu = 0{\cdot}15$; Conc, concentric; Ecc_b, eccentric at bottom; and Ecc_t, eccentric at top). —■—, Conc(x), Conc(y); —●—, $\text{Ecc}_b(x)$, $\text{Ecc}_b(y)$; —▲—, $\text{Ecc}_t(x)$, $\text{Ecc}_t(y)$; –·□–·, Conc(x&y); –·○–·, $\text{Ecc}_b(x\&y)$; –·△–·, $\text{Ecc}_t(x\&y)$.

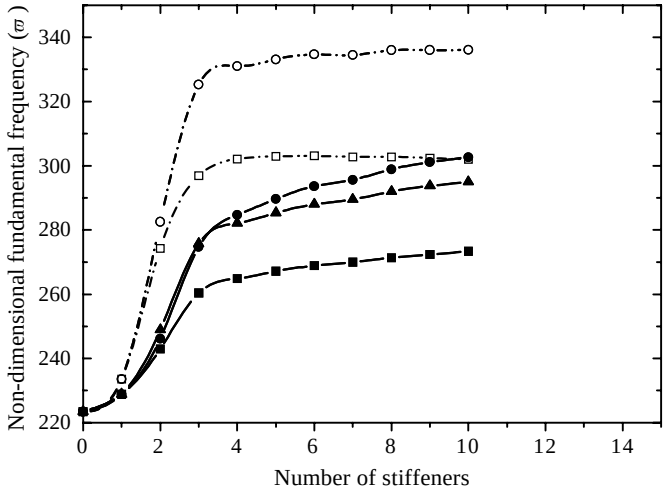

Figure 9. Variation of non-dimensional fundamental frequency of stiffened clamped hyperbolic paraboloid shell with respect to numbers, types and orientations of stiffeners ($\gamma = a/b = 1$, $b/h = 250$, $R_y/R_x = -1$, $R_y/b = 3$, $b_{st}/h = 2$, $d_{st}/h = 6$ and $\nu = 0{\cdot}15$; Conc, concentric, Ecc_b, eccentric at bottom; and Ecc_t, eccentric at top). —■—, Conc(x), Conc(y); —●—, $\text{Ecc}_b(x)$, $\text{Ecc}_t(y)$; —▲—, $\text{Ecc}_t(x)$, $\text{Ecc}_b(y)$; –·□–·, Conc(x&y); –·○–·, $\text{Ecc}_b(x\&y)$, $\text{Ecc}_t(x\&y)$.

3.1. NUMBERS, TYPES AND ORIENTATIONS OF STIFFENERS

The objectives of the examples of Sl. No. 1 of Table 5 are to study the influences with respect to their number, types and orientations on square and clamped shells of four forms. Results of ϖ from Figures 8–11 clearly show that the fundamental frequency is increasing with the increase in the number of stiffeners as normally expected. However, this increase, though considerable in some of the forms at the early stage, gradually becomes insignificant

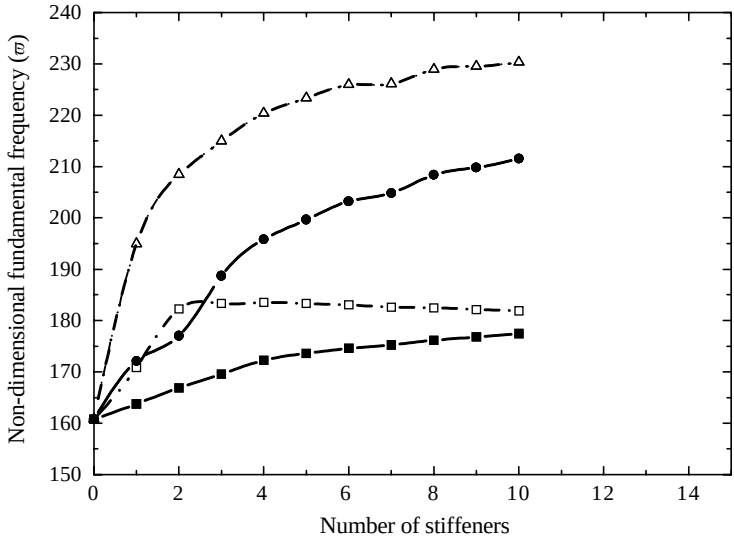

Figure 10. Variation of non-dimensional fundamental frequency of stiffened clamped hypar shell with respect to numbers, types and orientations of stiffeners ($\gamma = a/b = 1$, $b/h = 250$, $\Delta f/b = 0{\cdot}20$, $b_{st}/h = 2$, $d_{st}/h = 6$ and $\nu = 0{\cdot}15$; Conc, concentric, Ecc_b, eccentric at bottom; and Ecc_t, eccentric at top). —■—, Conc(x), Conc(y); —●—, $\text{Ecc}_b(x)$, $\text{Ecc}_t(x)$, $\text{Ecc}_b(y)$, $\text{Ecc}_t(y)$; – □ –, Conc(x&y); – · △ – ·, $\text{Ecc}_b(x\&y)$, $\text{Ecc}_t(x\&y)$.

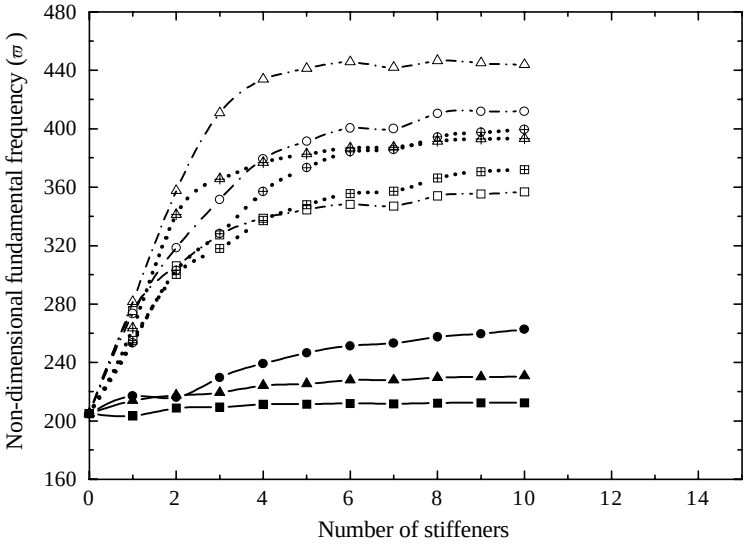

Figure 11. Variation of non-dimensional fundamental frequency of stiffened clamped conoidal shell with respect to numbers, types and orientations of stiffeners ($\gamma = a/b = 1$, $b/h = 250$, $(f_2 + \Delta f)/b = 0{\cdot}15$, $f_2/(f_2 + \Delta f) = 0{\cdot}25$, $b_{st}/h = 2$, $d_{st}/h = 6$ and $\nu = 0{\cdot}15$; Conc, concentric, Ecc_b, eccentric at bottom; and Ecc_t, eccentric at top). —■—, Conc(x); —●—, $\text{Ecc}_b(x)$; —▲—, $\text{Ecc}_t(x)$; ⋯ ⊞ ⋯, Conc(y); ⋯ ⊕ ⋯, $\text{Ecc}_b(y)$; ⋯ ⧋ ⋯, $\text{Ecc}_t(y)$; – · □ – ·, Conc(x&y), – · ○ – ·, $\text{Ecc}_b(x\&y)$; – · △ – ·, $\text{Ecc}_t(x\&y)$.

after a critical value of the number of stiffeners, as generally observed for all the four forms taken up here. A close look at the values of ϖ with the three types of stiffeners reveals the superiority of "eccentric at top" stiffeners for all the four clamped forms and then comes "eccentric at bottom", clearly indicating that the concentric stiffeners are much inferior in

all the four cases. Even, at least in one case of conoidal shell with one stiffener along the x direction proves to be worse than the unstiffened shell (Figure 11). However, this aspect will be taken up again while studying other results.

As regards the orientations of the stiffeners, orthogonal stiffeners having particular number show much higher ϖ than the same with an equal number of stiffeners either along the x or y direction, except in hyperbolic paraboloid shell (Figure 9), where the trend is just the opposite with two number of stiffeners. Between the remaining two orientations, y directional stiffeners establish their superiority to those along the x direction for the conoidal shell (Figure 11). For the elliptic paraboloid and hypar shells (Figures 8 and 10), the stiffeners along x and y directions are behaving in identical manner with having exactly the same value of ϖ, which is due to the symmetry of forms and stiffeners. Moreover, the "eccentric at top and bottom" stiffeners of the hypar shell yield the same result along any orientation due to the absence of curvatures along orthogonal directions (Figure 10). The same study for the hyperbolic paraboloid shell (Figure 9) reveals interesting features as mentioned below:

(1) In the case of the concentric stiffeners, the values of ϖ for stiffeners along the x direction are identical with those along the y direction, due to the symmetry.
(2) In the case of the eccentric stiffeners, however, all the values of ϖ along the x direction eccentric at bottom are equal to the respective values of ϖ along the y direction having eccentric at top and vice versa. But for the orthogonal stiffeners, the "eccentric at top and bottom" stiffeners behave in a similar manner.
(3) Up to four stiffeners, "eccentric at top and bottom" stiffeners along x and y directions show nearly the same trend. However, from four stiffeners onwards, the "eccentric at top" stiffeners are found to be more efficient than the "eccentric at bottom" ones along the y direction. Similarly, along the x direction, the stiffeners having eccentricity at bottom show superior performance than those having eccentricity at top.

The above discussion clearly establishes the better performance of orthogonal and eccentric at top stiffeners in majority of cases of clamped shells. Accordingly, the remaining examples of Sl. Nos. 2–4 of Table 5 are with orthogonal and eccentric at top stiffeners only.

3.2. BOUNDARY CONDITION AND ASPECT RATIO

A quick glance at the values of ϖ of Figures 12–15 clearly establishes the superiority of clamped shells when compared to the corresponding cases of simply supported ones for all three aspect ratios and for any particular number of orthogonal stiffeners considered here. For clamped stiffened shells, preference of the aspect ratio is 0·5, 1·0 and 2·0 for the higher enhancement of ϖ. Moreover, it should be observed carefully that simply supported elliptic paraboloid shell is not only the lowest ranker, it is also of concern as it indicates reduction of ϖ for any number of stiffeners particularly for the aspect ratios 2 and 1 (i.e., narrow and long, and square ones). It is, again, to be noted that for the aspect ratio of 0·5 (wide and short one), the stiffeners justify their presence in increasing the values of ϖ with respect to that of unstiffened ones (Figure 12). Hence, it is suggested that the narrow and long, and square elliptic paraboloid shells are not to be stiffened and preferably to be avoided. It is further seen from Figures 13–15 that in the three other shell forms of the simply supported case, the wide and short ones ($\gamma = 0{\cdot}5$) is the most efficient followed by the square ($\gamma = 1$) and then the narrow and long ones ($\gamma = 2$) similar to the clamped ones. The degree of superiority of clamped ones, though differs depending on the wide ranging combinations of three different aspect ratios and different number of stiffeners, is observed to be higher for the hypar shells

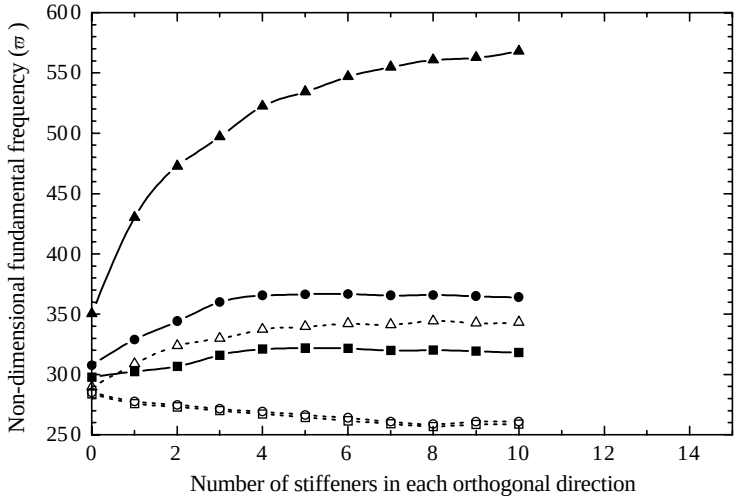

Figure 12. Variation of non-dimensional fundamental frequency of "eccentric at top" orthogonally stiffened elliptic paraboloid shell with respect to boundary conditions and aspect ratios ($b/h = 250$, $R_y/R_x = 1$, $R_y/b = 3$, $b_{st}/h = 2$, $d_{st}/h = 6$ and $v = 0{\cdot}15$; SS, simply supported; and CC, clamped). - - -□- - -, $\gamma = 2.0$ (SS); - - -○- - -, $\gamma = 1.0$ (SS); - - -△- - -, $\gamma = 0{\cdot}5$ (SS); —■—, $\gamma = 2{\cdot}0$ (CC); —●—, $\gamma = 1.0$ (CC); —▲—, $\gamma = 0{\cdot}5$ (CC).

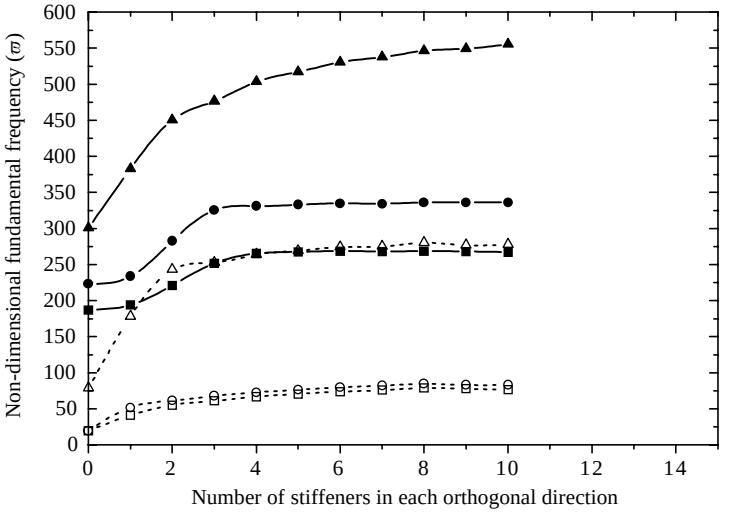

Figure 13. Variation of non-dimensional fundamental frequency of "eccentric at top" orthogonally stiffened hyperbolic paraboloid shell with respect to boundary conditions and aspect ratios ($b/h = 250$, $R_y/R_x = -1$, $R_y/b = 3$, $b_{st}/h = 2$, $d_{st}/h = 6$ and $v = 0{\cdot}15$; SS, simply supported; and CC, clamped). - - -□- - -, $\gamma = 2{\cdot}0$ (SS); - - -○- - -, $\gamma = 1{\cdot}0$ (SS); - - -△- - -, $\gamma = 0{\cdot}5$ (SS); —■—, $\gamma = 2{\cdot}0$ (CC); —●—, $\gamma = 1{\cdot}0$ (CC); —▲—, $\gamma = 0{\cdot}5$ (CC).

showing almost 6–7 times of increase of ϖ followed by conoidal shells (4–5 times of increase of ϖ) and then the hyperbolic paraboloid shells (2–3 times of increase of ϖ) and the lowest is the elliptic paraboloid shells (1·5–2 times of increase of ϖ). It is, therefore, recommended to use the clamped shells of any forms, followed by the three simply supported shell forms, i.e., hyperbolic paraboloid, hypar and conoidal, with aspect ratios 0·5, 1·0 and 2·0 in order of preference for stiffening.

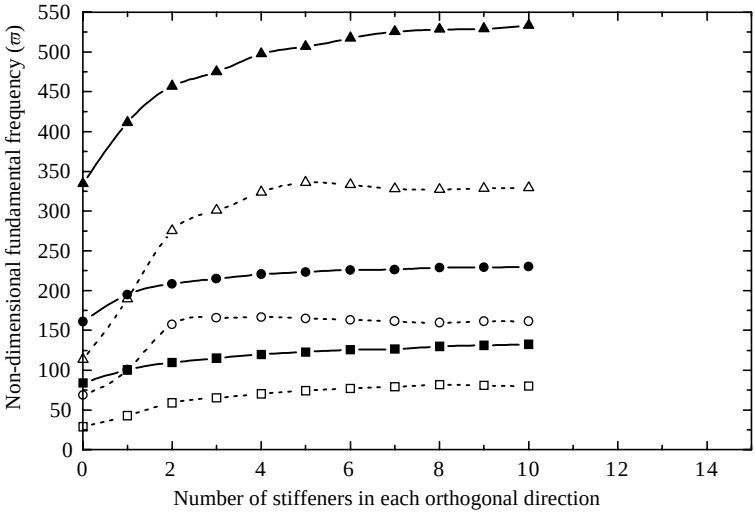

Figure 14. Variation of non-dimensional fundamental frequency of "eccentric at top" orthogonally stiffened hypar shell with respect to boundary conditions and aspect ratios ($b/h = 250$, $\Delta f/b = 0{\cdot}20$, $b_{st}/h = 2$, $d_{st}/h = 6$ and $\nu = 0{\cdot}15$; SS, simply supported; and CC, clamped). - - -□- - -, $\gamma = 2{\cdot}0$ (SS); - - -○- - -, $\gamma = 1{\cdot}0$ (SS); - - -△- - -, $\gamma = 0{\cdot}5$ (SS); —■—, $\gamma = 2{\cdot}0$ (CC); —●—, $\gamma = 1{\cdot}0$ (CC); —▲—, $\gamma = 0{\cdot}5$ (CC).

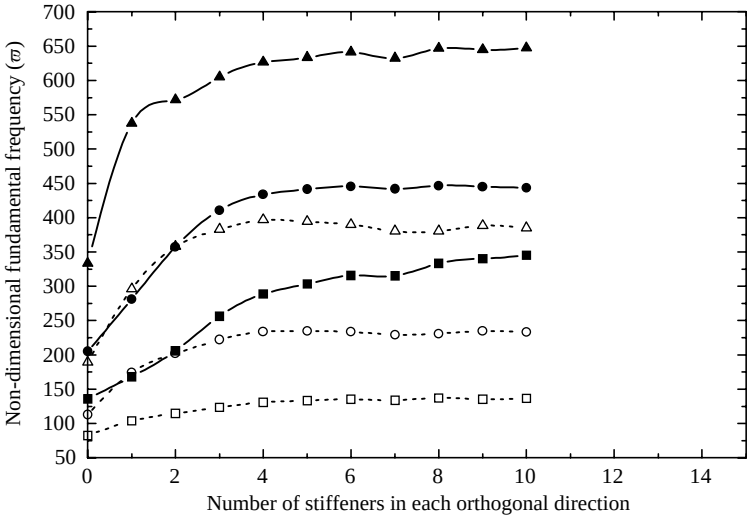

Figure 15. Variation of non-dimensional fundamental frequency of "eccentric at top" orthogonally stiffened conidial shell with respect to boundary conditions and aspect ratios ($b/h = 250$, $(f_2 + \Delta f)/b = 0{\cdot}15$, $f_2/(f_2 + \Delta f) = 0{\cdot}25$, $b_{st}/h = 2$, $d_{st}/h = 6$ and $\nu = 0{\cdot}15$; SS, simply supported; and CC, clamped). - - -□- - -, $\gamma = 2{\cdot}0$ (SS); - - -○- - -, $\gamma = 1{\cdot}0$ (SS); - - -△- - -, $\gamma = 0{\cdot}5$ (SS); —■—, $\gamma = 2{\cdot}0$ (CC); —●—, $\gamma = 1{\cdot}0$ (CC); —▲—, $\gamma = 0{\cdot}5$ (CC).

3.3. STIFFENER DEPTH TO SHELL THICKNESS RATIO (d_{st}/h)

Figures 16–19 display the values of ϖ for frequently preferred square, clamped, orthogonal and eccentric at top stiffened shells with increasing number of stiffeners and (d_{st}/h) ratios. The figures clearly show that for a specific shell thickness, the depth of stiffeners does not have a significant role particularly for lower number of stiffeners.

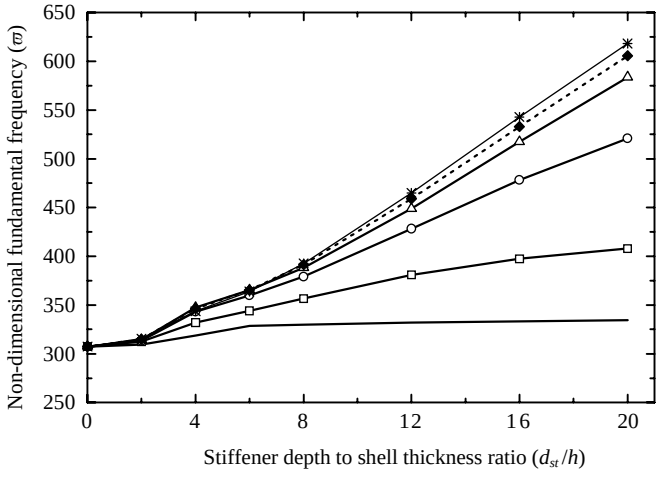

Figure 16. Variation of non-dimensional fundamental frequency of "eccentric at top" orthogonally stiffened clamped elliptic paraboloid shell with stiffener depth to shell thickness ratio ($\gamma = a/b = 1$, $b/h = 250$, $R_y/R_x = 1$, $R_y/b = 3$, $b_{st}/h = 2$ and $v = 0{\cdot}15$). ———, $n_x = n_y = 1$; —□—, $n_x = n_y = 2$; —○—, $n_x = n_y = 3$; —△—, $n_x = n_y = 4$; - - -◆- - -, $n_x = n_y = 7$; —∗—, $n_x = n_y = 10$.

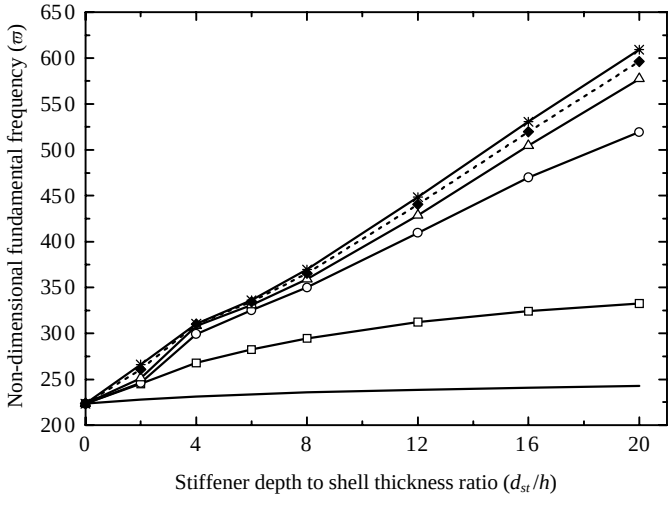

Figure 17. Variation of non-dimensional fundamental frequency of "eccentric at top" orthogonally stiffened clamped hyperbolic paraboloid shell with stiffener depth to shell thickness ratio ($\gamma = a/b = 1$, $b/h = 250$, $R_y/R_x = -1$, $R_y/b = 3$, $b_{st}/h = 2$ and $v = 0{\cdot}15$). ———, $n_x = n_y = 1$; —□—, $n_x = n_y = 2$; —○—, $n_x = n_y = 3$; —△—, $n_x = n_y = 4$; - - -◆- - -, $n_x = n_y = 7$; —∗—, $n_x = n_y = 10$.

However, with increasing number of stiffeners, the depth of stiffeners plays an important role. It is also to be kept in mind that the increase of ϖ, though appreciable when the number of stiffeners are increasing initially, is not that significant with the further increase after a specific number of stiffeners (say 4×4). It may be observed that almost 80–90% of ϖ is achieved with 4×4 stiffeners when compared with the identical stiffeners of 10×10 numbers. In such a situation, therefore, these figures will help in deciding the corresponding depth of stiffeners for a particular number and a specific thickness of the shell. Moreover, for

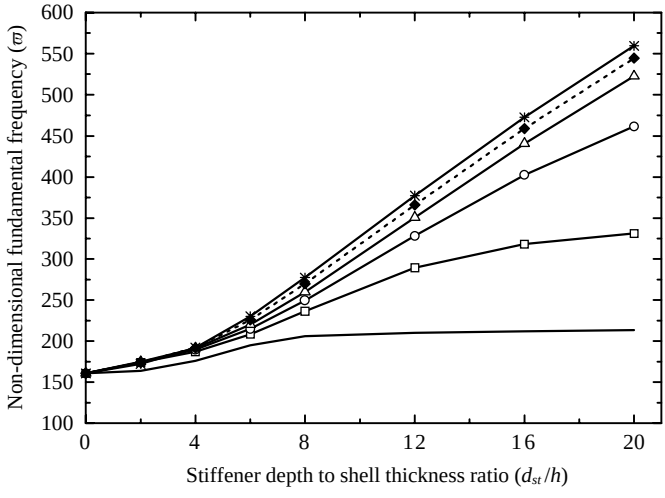

Figure 18. Variation of non-dimensional fundamental frequency of "eccentric at top" orthogonally stiffened clamped hypar shell with stiffener depth to shell thickness ratio ($\gamma = a/b = 1$, $b/h = 250$, $\Delta f/b = 0{\cdot}20$, $b_{st}/h = 2$ and $v = 0{\cdot}15$). ———, $n_x = n_y = 1$; —□—, $n_x = n_y = 2$; —○—, $n_x = n_y = 3$; —△—, $n_x = n_y = 4$; - - -◆- - -, $n_x = n_y = 7$; —*—, $n_x = n_y = 10$.

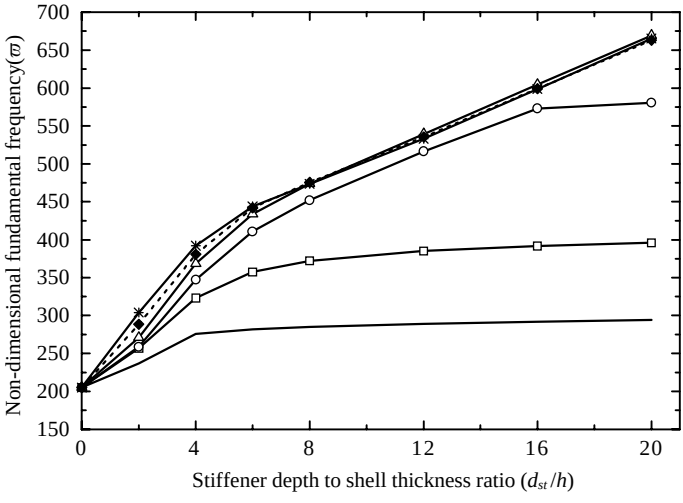

Figure 19. Variation of non-dimensional fundamental frequency of "eccentric at top" orthogonally stiffened clamped conoidal shell with stiffener depth to shell thickness ratio ($\gamma = a/b = 1$, $b/h = 250$, $(f_2 + \Delta f)/b = 0{\cdot}15$, $f_2/(f_2 + \Delta f) = 0{\cdot}25$, $b_{st}/h = 2$ and $v = 0{\cdot}15$). ———, $n_x = n_y = 1$; —□—, $n_x = n_y = 2$; —○—, $n_x = n_y = 3$; —△—, $n_x = n_y = 4$; - - -◆- - -, $n_x = n_y = 7$; —*—, $n_x = n_y = 10$.

specific values of both d_{st} and h, these figures will be useful in deciding the number of stiffeners in order to attain a desired value of ϖ.

Further, it is to be noted that for lower values of (d_{st}/h), the range of variations of ϖ is quite large for the clamped conoidal shell (Figure 19) followed by clamped hyperbolic paraboloid shell (Figure 17), while clamped elliptic paraboloid and hypar shells (Figures 16 and 18) show a narrow range. From this, the obvious preference of conoidal shell followed by hyperbolic paraboloid shell will dominate over the other two forms, i.e., elliptic paraboloid and hypar shells.

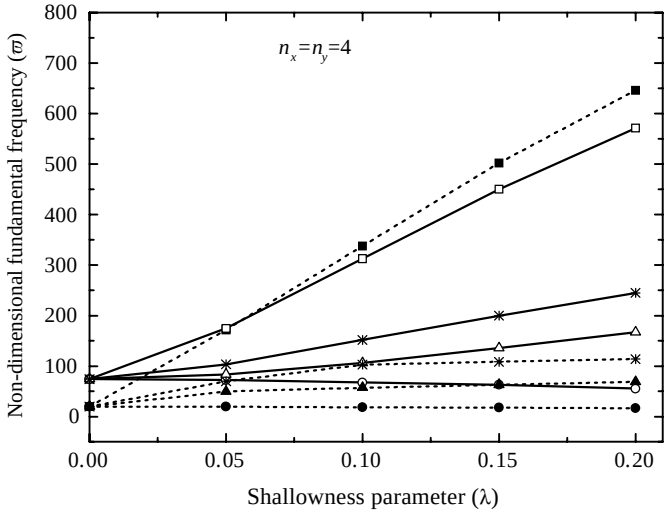

Figure 20. Variation of non-dimensional fundamental frequency of simply supported shells with/without "eccentric at top" orthogonal stiffeners with shallowness parameter ($\gamma = a/b = 1$, $b/h = 250$, $b_{st}/h = 2$, $d_{st}/h = 6$ and $\nu = 0{\cdot}15$; Unst., unstiffened; St., stiffened; EP, elliptic paraboloid; HP, hyperbolic paraboloid; Hyp, hypar and Con = conoidal). - - -■- - -, EP(Unst.); —□—, EP(St.); - - -●- - -, HP(Unst.); —○—, HP(St.); - - -▲- - -, Hyp(Unst.); —△—, Hyp(St.); - - -∗- - -, Con(Unst.); —∗—, Con(ST).

3.4. SHALLOWNESS PARAMETER (λ) OF THE SHELL

These examples, listed under Sl. No. 4 of Table 5, are taken up for frequently used square shell forms of simply supported and clamped boundary conditions with only 4×4, orthogonal and eccentric at top stiffeners and shallowness parameter varying from 0 to 0·2 (i.e., plate to shallow shell range). Figures 20 and 21 present ϖ for these cases along with those of unstiffened ones also.

Though, in general, it is observed that ϖ is increasing with increasing value of λ both for stiffened and unstiffened shells except in the case of simply supported hyperbolic paraboloid shell, where the situation is just the reverse (Figures 20 and 21). However, the rate of increase of ϖ with the increase of λ for all the forms in both boundary conditions are different as seen from the stiff and flat slope of these graphs. Figure 20 clearly shows that the simply supported elliptic paraboloid stiffened shells have lower ϖ than those without any stiffeners for λ beyond 0·05, though the absolute values of ϖ of this shell form for both stiffened and unstiffened ones are equally comparable to the clamped hyperbolic paraboloid and conoidal shells. In other shell forms with simply supported boundary conditions, there is no significant effect of λ on ϖ for both stiffened and unstiffened ones and the absolute values of ϖ are also much less. Figure 21 reveals the order of preference of the clamped shell forms with regard to the increase of ϖ in the entire range of λ, i.e., up to 0·2, as hyperbolic paraboloid, elliptic paraboloid and conoidal shells. It is further seen that the appreciable improvement of ϖ is observed for the hyperbolic paraboloid and conoidal stiffened shells when compared to the corresponding unstiffened ones. Figure 21 is thus useful in identifying a particular form with respect to the improvement of ϖ when other parameters are kept constant.

It is evident from the above study of the natures of ϖ for different combinations of shell forms, boundary conditions and other stiffener parameters that the increase of ϖ does not necessarily follow the accepted norm of increasing the stiffeners, etc. The situation is both

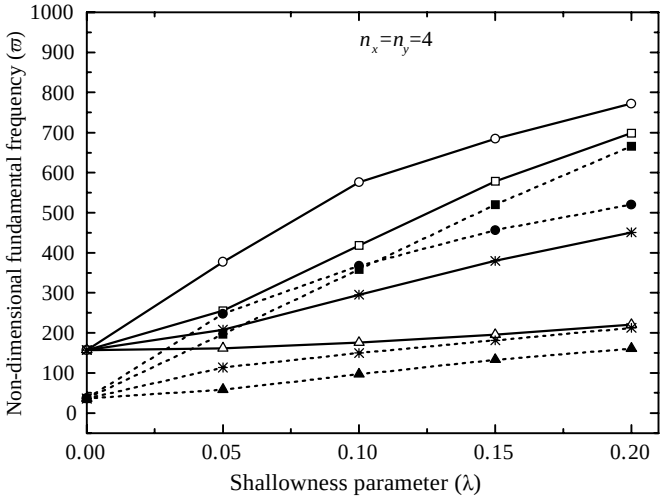

Figure 21. Variation of non-dimensional fundamental frequency of clamped shells with/without "eccentric at top" orthogonal stiffeners with shallowness parameter ($\gamma = a/b = 1$, $b/h = 250$, $b_{st}/h = 2$, $d_{st}/h = 6$ and $\nu = 0{\cdot}15$; Unst., unstiffened; St., stiffened; EP, elliptic paraboloid; HP, hyperbolic paraboloid; Hyp, hypar and Con = conoidal). - - -■- - -, EP(Unst.); —□—, EP(St.); - - -●- - -, HP(Unst.); —○—, HP(St.); - - -▲- - -, Hyp(Unst.); —△—, Hyp(St.); - - -∗- - -, Con(Unst.); —∗—, Con(ST).

complex and interactive. In some situations the reverse trend of decreasing ϖ with increasing either depth or number of stiffeners, etc. can be justified by the predominant "mass action" as both stiffness and mass play a significant role in determining the ϖ in an interactive mode.

4. CONCLUSION

A finite element analysis employing doubly curved isoparametric eight-/nine-node thin shallow element and curved isoparametric three-node beam element is carried out to study the free vibration characteristics of different doubly curved stiffened shallow shells for finding the suitability of stiffening. The accuracy of the formulation is established by comparing the present results with those available in the literature. Though the converged results of both the elements are nearly the same, the nine-node shell element establishes its superiority with respect to the rate of convergence.

The present study clearly reveals that the fundamental frequency of stiffened shallow shells for all the four forms is increasing with the increase of the number of stiffeners up to a specific number after which this increase gradually becomes insignificant. It is to be noted that almost 80–90% of fundamental frequency is achieved with 4×4 stiffeners when compared with the identical 10×10 stiffeners. Further, the eccentric stiffeners prove their superiority over concentric stiffeners with respect to dynamic stiffness for all the four forms considered here. In most of the cases, the shell with eccentric at top stiffener shows better performance than that with eccentric at bottom stiffeners. As regards the three orientations of the stiffeners, it is observed that the orthogonal stiffeners are the best followed by y directional stiffeners and then x directional stiffeners.

It is inferred that the clamped stiffened shallow shells show better performance than the simply supported ones with respect to dynamic stiffness for all the forms considered. With regard to the aspect ratios of the shells, the wide and short ones ($\gamma = 0{\cdot}5$) is the most efficient

followed by the square ($\gamma = 1{\cdot}0$) and the narrow and long ones ($\gamma = 2{\cdot}0$) for both the boundary conditions of all the four stiffened forms. It is also to be noted that the long and square elliptic paraboloid shells with simply supported boundary condition are preferably avoided for stiffening as the fundamental frequency of the stiffened ones is even lower than that of the unstiffened ones.

The non-dimensional fundamental frequency (ϖ) versus stiffener depth to shell thickness ratio (d_{st}/h) plots of the present study clearly show that the dynamic stiffness of frequently favoured square, orthogonal and eccentric at top stiffened shells of clamped boundary condition increases with the increase in the stiffener depth to shell thickness ratio. However, the range of increase in dynamic stiffness depends mainly on stiffener depth to shell thickness ratio, number of stiffeners and shell forms. Hence, these plots are useful in finding one parameter by keeping other two parameters fixed to attain a desired fundamental frequency. Moreover, the clamped hyperbolic paraboloid and conoidal shells are most suitable for stiffening unlike the other two forms as the considerable increase in fundamental frequency is observed for these forms due to addition of more number of stiffeners at the lower range of stiffener depth to shell thickness ratio (d_{st}/h), which may be preferred due to some practical constraints.

It is observed that the dynamic stiffness of simply supported elliptic paraboloid stiffened and unstiffened shells only can be improved by increasing the shallowness parameter (λ). However, the reduction of ϖ, though marginal, beyond $\lambda = 0{\cdot}2$ for the simply supported elliptic paraboloid stiffened shells clearly indicates the adoption of this shell without stiffeners. On the other hand, for all clamped stiffened shells, there is enough scope to improve the dynamic stiffness by increasing the shallowness parameter. The clamped hyperbolic paraboloid and conoidal stiffened shells are most suitable for stiffening due to their superior performance throughout the range of shallowness parameter taken up here. The ϖ versus λ plots of the present study for four forms of shells are useful in deciding one of the parameters, i.e., shallowness parameter/shell form, keeping the other constant to attain a desired dynamic stiffness.

REFERENCES

1. S. A. Rinehart and J. T. S. Wang 1972 *Journal of Sound and Vibration* **24**, 151–163. Vibration of simply supported cylindrical shells with longitudinal stiffeners.
2. D. J. Mead and N. S. Bardell 1986 *Journal of Sound and Vibration* **111**, 229–250. Free vibration of a thin cylindrical shell with discrete axial stiffeners.
3. D. J. Mead and N. S. Bardell 1987 *Journal of Sound and Vibration* **115**, 499–520. Free vibration of a thin cylindrical shell with periodic circumferential stiffeners.
4. B. A. J. Mustafa and R. Ali 1987 *Journal of Sound and Vibration* **113**, 317–327. Prediction of natural frequency of vibration of stiffened cylindrical shells and orthogonally stiffened curved panels.
5. B. A. J. Mustafa and R. Ali 1987 *Computers and Structures* **27**, 803–810. Free vibration analysis of multi-symmetric stiffened shells.
6. N. S. Bardell and D. J. Mead 1989 *Journal of Sound and Vibration* **134**, 29–54. Free vibration of an orthogonally stiffened cylindrical shell, Part I: discrete line simple supports.
7. N. S. Bardell and D. J. Mead 1989 *Journal of Sound and Vibration* **134**, 55–72. Free vibration of an orthogonally stiffened cylindrical shell, Part II: Discrete general stiffeners.
8. S. P. Cheng and C. Dade 1990 *Computers and Structures* **36**, 623–629. Dynamic analysis of stiffened plates and shells using spline Gauss collocation method.
9. M. L. Accorsi and M. S. Bennett 1991 *Journal of Sound and Vibration* **148**, 279–292. A finite element based method for the analysis of free wave propagation in stiffened cylinders.
10. Z. Mecitoglu and M. C. Dokmeci 1991 *AIAA Journal* **30**, 848–850. Free vibrations of a thin, stiffened, cylindrical shallow shell.

11. R. S. LANGLEY 1992 *Journal of Sound and Vibration* **156**, 521–540. A dynamic stiffness technique for the vibration analysis of stiffened shell structures.
12. P. S. RAO, G. SINHA and M. MUKHOPADHYAY 1993 *International Shipbuilding Progress* **40**, 261–292. Vibration of submerged stiffened plates by the finite element method.
13. G. SINHA and M. MUKHOPADHYAY 1994 *Journal of Sound and Vibration* **171**, 529–548. Finite element free vibration analysis of stiffened shells.
14. G. SINHA and M. MUKHOPADHYAY 1997 *Computers and Structures* **62**, 919–933. Static, free and forced vibration analysis of arbitrary non-uniform shells with tapered stiffeners.
15. J. JIANG and M. D. OLSON 1994 *Journal of Sound and Vibration* **173**, 73–83. Vibration analysis of orthogonally stiffened cylindrical shells using super finite elements.
16. A. J. STANLEY and N. GANESAN 1997 *Computers and Structures* **65**, 33–45. Free vibration characteristics of stiffened cylindrical shells.
17. B. SIVASUBRAMONIAN, G. V. RAO and A. KRISHNAN 1999 *Journal of Sound and Vibration* **226**, 41–55. Free vibration of longitudinally stiffened curved panels with cutout.
18. V. Z. VLASOV 1958 *Allgemeine Schalentheorie und ihre Anwendung in der Technik*. Berlin: Akademie Verlag.
19. O. C. ZIENKIEWICZ and R. L. TAYLOR 1991 *The Finite Element Method*, Vol. 2, 5. New York: McGraw-Hill Book Company; fourth edition.
20. A. DEB and M. BOOTON 1988 *Computers and Structures* **28**, 361–372. Finite element models for stiffened plates under transverse loading.
21. L. T. STAVRIDIS 1998 *Journal of Sound and Vibration* **218**, 861–882. Dynamic analysis of shallow shells of rectangular base.
22. M. D. OLSON and C. R. HAZELL 1977 *Journal of Sound and Vibration* **50**, 43–61. Vibration studies on some integral rib-stiffened plates.
23. A. MUKHERJEE and M. MUKHOPADHYAY 1988 *Computers and Structures* **30**, 1303–1317. Finite element free vibration of eccentrically stiffened plates.
24. A. BHIMARADDI, A. J. CARR and P. J. MOSS 1989 *Computers and Structures* **33**, 295–305. Finite element analysis of laminated shells of revolution with laminated stiffeners.

APENDIX A: NOMENCLATURE

A_{sx}	cross-sectional area of x-stiffener
a, b	length and width of shell
b_{st}, d_{st}	breadth and depth of stiffener respectively
$\{d\}$	eigenvector
E, E_{sx}	modulus of elasticity of shell and x-stiffener respectively
e_{sx}	eccentricity of x-stiffener with respect to the mid-surface of shell
f_1, f_2	central rise of edges of shells along x and y directions respectively
$f_2, f_2 + \Delta f$	lower and higher central rise of the edges of conoidal shell along the y direction respectively
G_{sx}	shear modulus of x-stiffener
h	thickness of the shell
I_{sx}, J_{sxe}	moment of inertia and equivalent polar moment of inertia of x-stiffener about the mid-surface of shell
$[K]$, $[K_e]$	global and element stiffness matrices of stiffened shell respectively
$[K_{she}]$	element stiffness matrix of the unstiffened shell
$[K_{xe}]$, $[K_{ye}]$	element stiffness matrices of x-stiffener and y-stiffener respectively
k_x, k_y, k_{xy}, k_{xz}, k_{yz}	curvatures of shell
$[M]$, $[M_e]$	global and element mass matrices of the stiffened shell respectively
$[M_{she}]$	element mass matrix of the unstiffened shell
$[M_{xe}]$, $[M_{ye}]$	element mass matrices of x-stiffener and y-stiffener respectively
M_x, M_y, M_{xy}	internal moment resultants of shell per unit length
M_{sxx}	internal moment resultants of x-stiffener per unit length
N_i, $N_{\xi i}$, $N_{\eta i}$	shape functions of the shell, x- and y-stiffener element
N_x, N_y, N_{xy}	internal in-plane force resultants of shell per unit length
N_{sxx}	internal in-plane force resultant of x-stiffener per unit length
n_x, n_y	number of stiffeners along x and y directions respectively
Q_{xz}, Q_{yz}	internal transverse shear resultants of shell per unit length

Q_{sxz}	internal transverse shear resultant of x-stiffener per unit length
R_x, R_y	radii of curvature of the shell along x and y directions respectively
R_{xy}	twist radius of curvature
S_{sx}	first moment of cross-sectional area of x-stiffener about the mid-surface of shell
T_{sxx}	internal torsion resultant of x-stiffener
u_i, v_i, w_i	displacements of the shell element at a node i along x-, y- and z-axis respectively
u_{sxi}, w_{sxi}	displacements of the x-stiffener element at a node i along x- and z-axis respectively
v_{syi}, w_{syi}	displacements of the y-stiffener element at a node i along y- and z-axis respectively
X, Y, Z	global Cartesian co-ordinate axes
x, y, z	local Cartesian co-ordinate axes
α_i, β_i	rotation of the shell element at a node i along x- and y-axis respectively
α_{sxi}, β_{sxi}	rotation of the x-stiffener element at a node i along x- and y-axis respectively
α_{syi}, β_{syi}	rotation of the y-stiffener element at a node i along x- and y-axis respectively
$\{\delta_{sxi}\}$, $\{\delta_{syi}\}$	displacement components of x-stiffener and y-stiffener respectively
$\{\varepsilon\}$, $\{\varepsilon_{sx}\}$	strain components of the shell and x-stiffener element respectively
ε_x^0, ε_y^0, γ_{xy}^0	in-plane strains of the mid-surface of the shell
γ	aspect ratio of the shell
γ_{xz}^0, γ_{yz}^0	transverse strains of the mid-surface of the shell
λ	shallowness parameter of the shell
ν	the Poisson ratio
ρ, ρ_{sx}	mass density of the shell and x-stiffener respectively
ϖ	non-dimensional fundamental frequency
ω	fundamental frequency in rad/s
ξ, η	local natural co-ordinates of a shell element